Chemical failure modes of AlQ3-based OLEDs: AlQ3 hydrolysis

John E. Knox,† Mathew D. Halls, Hrant P. Hratchian‡ and H. Bernhard Schlegel*

Received 20th October 2005, Accepted 13th February 2006
First published as an Advance Article on the web 24th February 2006
DOI: 10.1039/b514898g

Tris(8-hydroxyquinoline)aluminum(III), AlQ3, is used in organic light-emitting diodes (OLEDs) as an electron-transport material and emitting layer. The reaction of AlQ3 with trace H_2O has been implicated as a major failure pathway for AlQ3-based OLEDs. Hybrid density functional calculations have been carried out to characterize the hydrolysis of AlQ3. The thermochemical and atomistic details for this important reaction are reported for both the neutral and oxidized $AlQ3/AlQ3^+$ systems. In support of experimental conclusions, the neutral hydrolysis reaction pathway is found to be a thermally activated process, having a classical barrier height of 24.2 kcal mol^{-1}. First-principles infrared and electronic absorption spectra are compared to further characterize AlQ3 and the hydrolysis pathway product, AlQ2OH. The activation energy for the cationic AlQ3 hydrolysis pathway is found to be 8.5 kcal mol^{-1} lower than for the neutral reaction, which is significant since it suggests a role for charge imbalance in promoting chemical failure modes in OLED devices.

Introduction

Organic light emitting diodes (OLEDs) are currently under intense investigation for applications in next generation display technologies.[1,2] OLEDs are heterojunction devices in which organic active layers are incorporated into devices as thin solid films. These devices are normally composed of at least one hole-transport layer and one electron-transport layer forming an organic/organic heterojunction. Holes from the anode and electrons from the cathode travel through the transport layers until they form a singlet exciton that relaxes giving rise to electroluminescence. The organic materials are chosen with close regard to their electronic energy levels, usually such that the electrons are confined to the electron-transport layer which, upon injection of holes, also acts as the emitting layer.

Research into organic materials for use in OLEDs has mostly focused on conjugated polymers[3,4] or low molecular weight materials.[5] In 1987 Tang and VanSlyke reported an efficient OLED using tris-(8-hydroxyquinoline)-aluminum (AlQ3) as the electron-transport layer and emitting material.[6] Since then, metal-quinolates have become standard electroluminescent materials for these devices, with AlQ3 being the most widely studied.[7] From a theoretical standpoint, numerous studies have been carried out examining the properties of AlQ3 directly related to its role in OLED devices; including the mechanism of charge transport[8] and the nature of the excited electronic states giving rise to device emission.[9–12]

Department of Chemistry and Institute for Scientific Computing, Wayne State University, Detroit MI, 48202, USA. E-mail: hbs@chem.wayne.edu
† Present address: Novartis Institute for Tropical Diseases, 10 Biopolis Road, #05-01 Chromos, Singapore 138670.
‡ Present address: Raghavachari group, Department of Chemistry, Indiana University, Bloomington, IN, 47405, USA.

Despite showing excellent device characteristics, full realization of this technology has been hampered due to a lack of device stability. OLEDs incorporating AlQ3 suffer from device degradation due to localized chemical failure and from a long-time intrinsic degradation in performance. Numerous causes of OLED device degradation have been reported in the literature, many being related to electrode materials such as the delamination of electrodes,[13] cathode oxidation[14] or electrochemical reactions at the electrode/organic interfaces.[15] These failure modes have largely been controlled by judicious choice of electrode metal and device architecture. Additional failure modes have been proposed that are directly related to the chemistry and properties of the AlQ3 layer used in the OLED devices. Popovic and co-workers[16] have attributed the long-term device degradation of AlQ3-based OLEDs to an intrinsic instability of the AlQ3 cation, which is formed due to an imbalance of charge at the heterojunction. A prevalent chemical failure pathway involves the hydrolysis of AlQ3 due to moisture contamination.

Papadimitrakopoulos and co-workers[17–19] first suggested that one of the major local failure modes for OLEDs incorporating AlQ3, is due to reaction with trace H_2O, liberating 8-hydroxyquinoline and producing a hydroxylated aluminum quinolate, AlQ2OH. The released 8-hydroxyquinoline is thought to react further, yielding a nonemissive oxidative condensation product that quenches luminescence. Experimental observations using thermogravimetric analysis, gas chromatography-mass spectroscopy (GC-MS), infrared absorption and electronic absorption support the ready solid phase hydrolysis of AlQ3 exposed to air at elevated operating temperatures.[17–19] Recently, additional experimental evidence, obtained using AFM and acoustic sensing, implicate a reaction with H_2O in the degradation of AlQ3 thin films, showing both a change in film morphology and composition.[20,21]

Given the central role AlQ3 plays in academic and industrial OLED research, it is crucial to develop an understanding of

the thermochemistry and mechanism of the competing local chemical failure pathways. In the present work, we report a first attempt to examine the initial reaction step in the proposed chemical failure mode for AlQ3-based OLEDs due to the hydrolysis by trace amounts of water. First-principle calculations based on hybrid density functional theory are carried out for the reaction between AlQ3 and H_2O to investigate the energetics and atomistic details of the hydrolysis reaction pathway. Calculations are carried out for the neutral and cationic AlQ3 species for comparison, to examine the effect of local charge imbalance on chemical reactivity. Also, an estimate of the changes in AlQ3 stability due to the condensed phase environment of the thin film layer comprising an OLED is obtained using a polarizable continuum model.

Methods

The calculations described here were carried out using the Gaussian suite of programs,[22] using the B3-PW91 hybrid density functional, which corresponds to Becke's three-parameter exchange functional (B3)[23] with Perdew and Wang's gradient-corrected correlation functional (PW91).[24] For ground state calculations, the standard Pople double-ξ basis set plus polarization was employed, denoted 6-31G(d).[25,26] Full geometry optimizations were carried out for the reactants, transition structure and product species followed by subsequent harmonic frequency calculations, which verified the nature of the respective critical points and yielded zero-point energy (ZPE) corrections. In this work, all reported enthalpies include ZPE. The location of the transition state was determined by an extensive search using methods such as QST2.[27] More accurate reaction energetics were computed with the B3-PW91 functional and the 6-311+G(d,p) basis set[28,29] using the B3-PW91/6-31G(d) optimized geometries. The use of the larger basis set changed the relative energies by 2–4 kcal mol^{-1}. Basis set superposition corrections are expected to be *ca.* 1 kcal mol^{-1} or less, and were not included in the present calculations. The electronic absorption spectra for AlQ3 and AlQ2OH were obtained using time-dependent density functional (TD-DFT) calculations, using the B3-PW91 functional.[30] As in our previous study of the emissive excited state of AlQ3,[9] the 3-21+G* basis set was employed for the TD-B3-PW91 calculations.[25,26] Condensed phase calculations were carried out using a conductor-like polarizable continuum model (CPCM),[31,32] for comparison with the gas phase results.

Results and discussion

AlQ3 has become the archetype electron-transport and emitting layer in low molecular weight OLEDs, giving rise to devices with a characteristic green electroluminescence (λ = 519 nm).[7] Experimental studies of the absorption and luminescence spectra of AlQ3 comparing results from solution and thin solid films indicate that the low-energy excited states of these materials are localized on individual molecular sites.[33] This is highly encouraging, suggesting that valuable insight might be obtained from gas phase molecular calculations. AlQ3 has two geometric isomers, the facial (*fac*-AlQ3) and meridianal (*mer*-AlQ3) forms having C_3 and C_1 symmetries, respectively. Experimental and theoretical studies indicate that *mer*-AlQ3 is the dominant form. Sheppard and co-workers[34] were unable to detect resonances from *fac*-AlQ3 during proton NMR measurements of AlQ3. Additionally, Kafafi and co-workers[35] carried out a low temperature matrix isolation infrared study of AlQ3 and found little or no evidence for the presence of the facial isomer. Computational studies have shown that *mer*-AlQ3 is the most stable geometric isomer. Curioni *et al.*[36] carried out calculations using the gradient-corrected density functional, B-LYP, and a plane wave/pseudopotential basis on both isomers of AlQ3 and found that *mer*-AlQ3 was *ca.* 4 kcal mol^{-1} lower in energy than the facial isomer. Kafafi and co-workers,[35] found that the *mer*-isomer was preferred by an even larger amount. Their results using the hybrid density functional, B3-LYP, and the SDD basis set puts *mer*-AlQ3 *ca.* 8 kcal mol^{-1} lower in energy then *fac*-AlQ3. Therefore, the present work will consider *mer*-AlQ3 exclusively.

Neutral AlQ3 hydrolysis

The *mer*-AlQ3 structure consists of a central Al atom (+3 formal oxidation state) surrounded by three quinolate ligands in a pseudooctahedral configuration. Each of the three ligands are bidentate coordinating to the metal centre through a pendent hydroxyl oxygen, with loss of H, and a skeletal nitrogen and are not equivalent, each being denoted as a-, b- and c-quinolate. The structure is such that the a- and c-quinolate nitrogens and the b- and c-quinolate oxygens are *trans* to each other, being connected to the *fac*-AlQ3 isomer through the flipping of the c-quinolate ligand. In the current study, the geometry of *mer*-AlQ3 was computed at the B3-PW91/6-31G(d) level of theory. The ground-state structure of AlQ3 has been studied extensively by a number of groups and the results of the present calculations are in excellent agreement with previous theoretical determinations[35–40] and experimental measurements.[41,42] The bond distances of the inner coordination sphere are given in Table 1, and are within 0.02 Å of previous high level calculations[9] and within <0.035 Å of X-ray determinations. The orbital energies for *mer*-AlQ3 computed at the B3-PW91/6-31G(d) level of theory are -5.43, -5.33 and -5.10 eV and -1.83, -1.59 and -1.51 eV for the HOMO and LUMO triplets, respectively. The dipole moment is calculated to be 4.46 D, which is comparable, but slightly lower than 5.30–5.51 D, reported in previous studies.[9,40]

Of the proposed chemical failure pathways for AlQ3-based OLEDs, the degradation of AlQ3 through reaction with ambient moisture remains one of the most likely processes. In AlQ3 hydrolysis, monomers composing the active film encounter trace H_2O and are thought to react according to a ligand-exchange mechanism, replacing one or more of the quinolates ligands with a hydroxyl group (AlQ2OH), and releasing a free 8-hydroxyquinoline ligand (HQ), as shown in Scheme 1. Both reaction products are then available to undergo further reaction within the matrix, producing final products that can degrade OLED device performance by depletion of emissive sites and/or production of species that quench luminescence. In experiments directly measuring the amount of

Table 1 Critical structure bond lengths for the inner coordination sphere of neutral and cationic *mer*-AlQ3 and reaction enthalpies calculated at the B3-PW91/6-31G(d) level of theory

		Inner coordination sphere bond lengths/Å						H_2O bond lengths/Å			
		RAl–N_a	RAl–N_b	RAl–N_c	RAl–O_a	RAl–O_b	RAl–O_c	RAl–O	RO–H^1	RO–H^2	E_{Rel}[a]/kcal mol^{-1}
Neutral AlQ3											
AlQ3 + H_2O	R	2.07	2.06	2.11	1.85	1.88	1.88	—	0.97	0.97	0.0
AlQ3···H_2O	RC	2.07	2.05	2.11	1.87	1.87	1.89	3.74	0.97	0.97	–5.3
[AlQ2-Q_a···H^1–OH^2]$^{\neq}$	TS	2.05	2.05	2.28	2.44	1.90	1.92	2.08	1.01	0.97	24.2
AlQ2OH···HQ	PC	2.19	2.09	2.14	3.31	1.86	1.88	1.80	1.48	0.96	9.1
AlQ2OH + HQ	P	—	2.05	2.09	—	1.83	1.83	1.74	—	0.96	11.4
Cationic AlQ3											
$AlQ3^+$ + H_2O	R	2.10	2.05	2.04	1.91	1.89	1.84	—	0.97	0.97	0.0
$AlQ3^+$···H_2O	RC	2.09	2.06	2.05	1.90	1.90	1.85	4.14	0.97	0.98	–3.4
[AlQ2-Q_a^+···H^1–OH^2]$^{\neq}$	TS	2.07	2.04	2.18	2.31	1.94	1.89	2.15	0.99	0.97	15.7
$AlQ2OH^+$···HQ	PC	2.27	2.03	2.05	3.38	1.83	1.84	1.93	1.01	0.97	4.5
$AlQ2OH^+$ + HQ	P	—	2.07	2.05	—	1.85	1.87	1.72	—	0.96	22.0

[a] Relative energies with respect to separated reactants calculated using B3-PW91/6-311+G(d,p) energies at the B3-PW91/6-31G(d) optimized geometries and corrected for zero point energy at the B3-PW91/6-31G(d) level.

released HQ upon exposure of AlQ3 to H_2O, no detectable signal was found for temperatures below 90 °C (363 K), suggesting a thermally activated process.[18] In this work, the initial AlQ3 hydrolysis reaction pathway is characterized according to five critical point structures: the separated reactants (R), reactant encounter complex (RC), the transition state (TS), the product channel complex (PC) and finally the separated product species (P).

As H_2O approaches AlQ3, it forms a reactant-like AlQ3···H_2O complex. Numerous binding configurations between AlQ3 and H_2O were evaluated and only the lowest energy structure is presented here. The AlQ3···H_2O complex is strongly stabilized compared to the separated reactants due to two hydrogen bond interactions with the lone pair electrons of the oxygens in the a- and c-quinolate ligands. The minimum energy configuration for the reactant complex is shown in Fig. 1a, with the AlQ3 inner coordination sphere and H_2O reactant atoms rendered to increase clarity. Bond lengths and relative energies for the AlQ3···H_2O complex and for the separated reactants are presented in Table 1. In this work, all reported reaction enthalpies include zero-point energy (ZPE) corrections. The reactant complex has a binding energy of 5.3 kcal mol^{-1}. The bond lengths listed in Table 1 indicate that formation of the reactant complex has little effect on the structural parameters. The reactant complex has an AlQ3···H_2O Al–O bond length of 3.74 Å and $H^{1/2}$–$O_{a/c}$ lengths of 2.23 and 1.95 Å, for the a- and c-quinolate, respectively.

Previous studies have examined the binding of alkali atoms with AlQ3 using density functional methods. Calculations by Curioni and Andreoni[37] using the gradient-corrected B-LYP density functional gave a binding energy of 11.0 kcal mol^{-1} for Ca interacting with *mer*-AlQ3, comparable to that found here for H_2O.

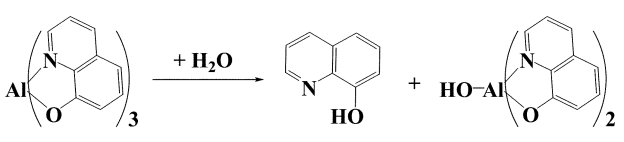

AlQ3 HQ AlQ2OH

Scheme 1

Following association of H_2O with the AlQ3, the system can evolve along the hydrolysis failure pathway. The reaction energy profile for the AlQ3 hydrolysis reaction is shown in Fig. 2 (critical structure energies denoted by ○). The relative reaction enthalpies for AlQ3 hydrolysis are listed in Table 1, along with inner coordination sphere bond lengths for the critical point structures. As illustrated there, the overall hydrolysis reaction is calculated to be endothermic, with the reaction products being higher in energy than the separated reactants by 11.4 kcal mol^{-1}. The structure of the activated complex for the process is shown in Fig. 1b (with dashed lines indicating transitional bonds). As expected, the AlQ3 hydrolysis pathway transition state has Al–O_a and H_2O O–H^1 bonds elongated by 0.57 and 0.04 Å compared to the AlQ3···H_2O reactant complex structural parameters, consistent with the ultimate breaking of these bonds. The Al–O distance decreases throughout the reaction from 3.74 Å in the reactant complex, becoming 2.08 Å in the transition state, and the final product structure has an Al–O bond length of 1.74 Å indicating completed Al–O bond formation. The process is found to be thermally activated with a classical barrier height for the AlQ3 hydroxylation pathway of 24.2 kcal mol^{-1}. Previously, Papadimitrakopoulos and co-workers[18] carried out a series of GC-MS experiments to investigate the hydrolytic thermal stability of AlQ3 and obtain an estimate of the activation energy for the AlQ3 hydrolysis reaction pathway. They measured an approximate activation energy of 16.3–22.5 kcal mol^{-1} for sublimed and annealed AlQ3 films, which is comparable to the calculated barrier height reported here. Related calculations on the hydrolysis of diethyl zinc show that a second molecule of water participating in the transition state will lower the enthalpy of the barrier but raise the free energy of the barrier.[43] The energy of the product species is stabilized in the product channel through formation of an AlQ2OH···HQ complex which is 15.1 and 2.3 kcal mol^{-1} lower in energy than the transition state and separated products for this reaction. The final product is shown in Fig. 1c.

It has been suggested that the AlQ2OH product may further react to form oxygen linked AlQ2 dimers, thereby regenerating H_2O which can further hydrolyze the AlQ3 active layer.[17–19]

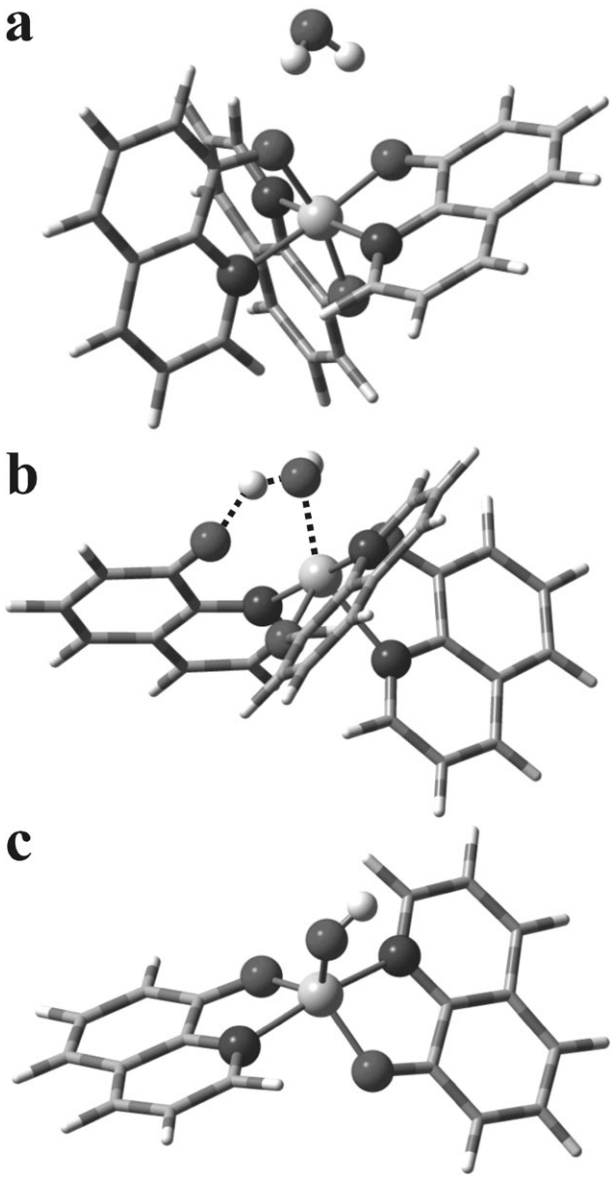

Fig. 1 The B3-PW91/6-31G(d) optimized structures of (a) the initial $H_2O\cdots AlQ3$ reactant complex, (b) the transition structure for the AlQ3 hydrolysis pathway, and (c) the final AlQ2OH product of AlQ3. (For clarity, inner coordination sphere atoms are rendered in spheres with rest as tubes. Transitional bonds are dashed.)

However at low moisture levels, it is possible that isolated AlQ2OH is formed in the matrix. Structural evidence for the AlQ3 hydrolysis pathway may be obtained using vibrational absorption spectroscopy. Xu and Xu have published a combined AFM, X-ray and infrared (IR) study of the effect of moisture exposure on AlQ3 thin solid films.[21] They did not report a detailed analysis, but conclude that a "handful of vibration intensities and modes" are affected by H_2O exposure and limited their measurements to the wavenumber range from 700 to 1800 cm^{-1}.

Work by Halls and Schlegel[44] has shown that hybrid density functional methods (*e.g.*, B3-PW91) perform very well in predicting quantitative infrared intensities and scaled harmonic frequencies. Kafafi and co-workers,[35] used hybrid DFT in their study of the low-temperature IR study of AlQ3, obtaining excellent agreement with matrix infrared measurements, which allowed the definitive assignment of observed bands. Fig. 3 shows the calculated infrared spectra in the fingerprint region ($< \sim 1700$ cm^{-1}) for AlQ3 and the hydrolysis pathway product, AlQ2OH. For clarity, the IR spectrum for AlQ3 is shown as absorption (upper trace) and the AlQ2OH IR is shown as transmission (lower trace). The calculated IR spectra were constructed using the scaled (0.9573)[45] theoretical vibrational frequencies and computed intensities by representing the IR bands by Gaussian lineshapes with a full width at half maximum (FWHM) of 4 cm^{-1}. Comparison of the spectra in Fig. 3, indicates that the IR spectrum is largely conserved between reactant and product. Notable however are the bands of significant intensity in the region around 700 cm^{-1}, which is known to be associated with the out-of-plane and torsional modes. AlQ3 shows only two bands with substantial intensity,

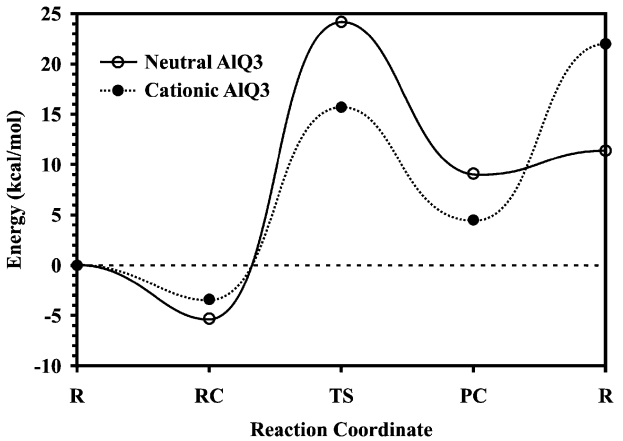

Fig. 2 Reaction energy profile for the reaction of neutral and cationic AlQ3 with H_2O at the a-quinolate ligand calculated at the B3-PW91/6-311+G(d,p)//B3-PW91/6-31G(d) level of theory, denoted ○ and ●, respectively.

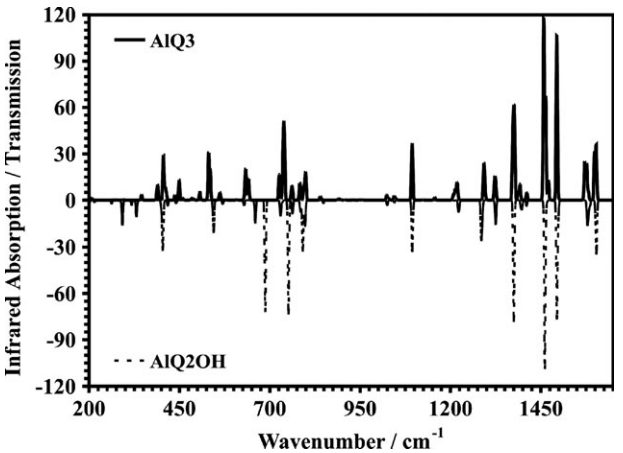

Fig. 3 Infrared spectrum of AlQ3 (upper trace, as absorption) along with that of the hydrolysis product AlQ2OH (lower trace, as transmission) for comparison, calculated at the B3-PW91/6-31G(d) level of theory.

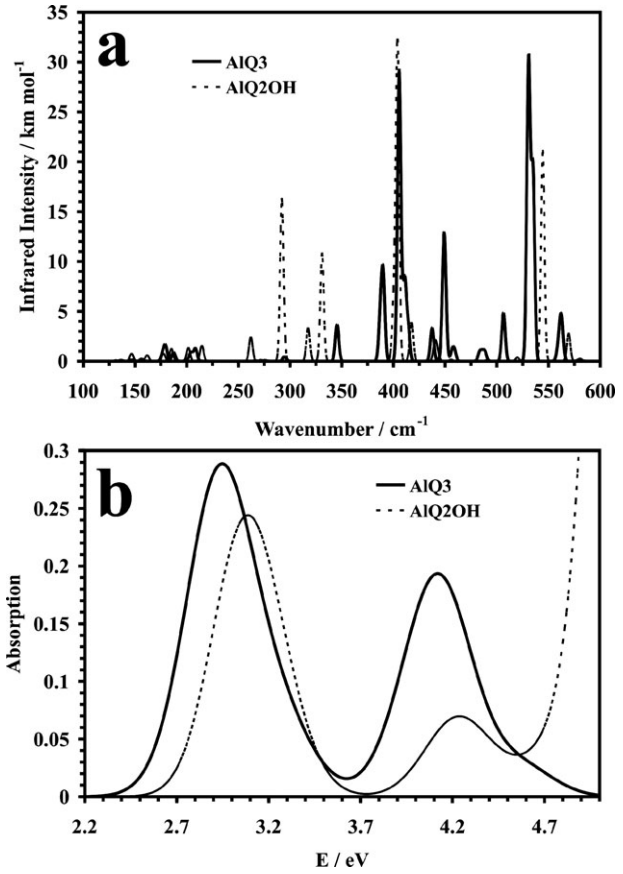

Fig. 4 (a) Infrared spectra for AlQ3 and AlQ2OH in the far-IR region, overlaid for comparison, calculated at the B3-PW91/6-31G(d) level of theory. (b) Electronic absorption spectra of AlQ3 and AlQ2OH calculated using TD-B3-PW91/3-21+G*.

whereas AlQ2OH shows three bands. This difference is largely attributable to the appearance of a new band at 688 cm^{-1} which can be assigned to the Al–OH bend and whose observation would be indicative of the AlQ3 hydrolysis pathway. Further characteristic differences can be seen, considering only the far-IR region which is shown in Fig. 4a. There the AlQ3 and AlQ2OH theoretical IR are overlaid for comparison. As shown there, AlQ2OH is predicted to have a band at 292 cm^{-1} of significant intensity, in a region free of AlQ3 resonances. This normal mode can be assigned to an Al–OH torsional mode, which again is a characteristic probe of AlQ2OH.

To provide a comparison of the electronic absorption spectra for AlQ3 and AlQ2OH, time-dependent density functional theory (TD-DFT) was used to compute the first twenty vertical excitations at the optimized equilibrium geometry. Previously, TD-DFT was used to extensively investigate the excited states of AlQ3.[9,40] Fig. 4b, shows the calculated absorption spectra for AlQ3 and AlQ2OH. The $S_0 \rightarrow S_1$ electronic transition for AlQ3 is computed to be 2.95 eV, which is intermediate to the previous theoretical determinations of 2.90 and 3.0 eV, using the TD-B3-LYP/3-21+G**[9] and TD-B3-LYP/6-31G(d)[40] levels of theory. Experimentally, this transition is observed at 3.18 eV (390 nm)[46] and can be assigned unambiguously to ^1L_a excited state of the 8-hydroxyquinoline.[47,48] Two critical differences can be observed between the AlQ3 and AlQ2OH traces in Fig. 4b. For AlQ2OH, the first absorption peak has an oscillator strength decreased by 17% compared to AlQ3. Additionally, the band edge and peak position is blue-shifted by 0.14 eV for AlQ2OH. Since the spectral shift is opposite that required to increase the overlap between the emission envelope of AlQ3 and the absorption of hydrolysis product, this seems to indicate that the species responsible for luminescence quenching in aged AlQ3-based OLEDs is the condensation product formed by *further* reactions of the liberated AlQ3 hydrolysis products.

Cationic AlQ3 hydrolysis

There is a growing consensus that one factor leading to the chemical failure of low molecular weight OLEDs is an imbalance of charge carriers in one of the transport layers composing the device.[49] Experiments carried out by Aziz *et al.*[16] suggest that for AlQ3-based devices, degradation is related to an imbalance of charge on the AlQ3 side of the heterojunction; resulting in the build-up of cationic AlQ3 species which may be less stable and more reactive than the pristine material. This is consistent with known approaches to extending AlQ3-OLED device lifetime, involving the introduction of charge injection layers to limit carrier transport.[50] Cationic AlQ3 may be more susceptible to chemical reactions such as the hydrolysis failure pathway. To examine this possibility, calculations were carried out for the $AlQ3^+ + H_2O$ reaction at the B3-PW91/6-31G(d) level of theory, for comparison with the neutral results.

The unbalanced injection of a hole across the heterojunction into the AlQ3 electron-transport layer would result in the oxidation of an AlQ3 monomer giving a cationic AlQ3 species. The cationic molecular structure of *mer*-AlQ3 has been studied previously using density functional theory[36] and the results reported here are comparable; predicting similar structural changes. The bond distances of the inner coordination sphere are given in Table 1, for comparison with those of the neutral. As seen there, oxidation of *mer*-AlQ3 results in a change in the Al–N and Al–O distances for the a-, b- and c-quinolates of +0.02 and +0.06, −0.01 and +0.01, and −0.07 and −0.04, respectively. Comparison of the B3-PW91/6-31G(d) total energies for the neutral and cationic AlQ3 structures gives an ionization potential (IP) of 6.32 eV. This value is in reasonable agreement with experimental measurements which report the IP of AlQ3 to be ~6 eV.[51,52]

As with neutral AlQ3, H_2O approaches the $AlQ3^+$ and forms a reactant-like $AlQ3^+\cdots H_2O$ complex. Bond lengths and relative energies for the $AlQ3^+\cdots H_2O$ complex and for the separated reactants are presented in Table 1. The cation reactant complex is calculated to have a binding energy of −3.4 kcal mol^{-1}, which is 1.9 kcal mol^{-1} less stable than the neutral complex. The cationic reactant complex has an $AlQ3^+\cdots H_2O$ Al–O bond length of 4.14 Å which is elongated by 0.4 Å from the neutral structure.

The reaction energy profile for the $AlQ3^+$ hydrolysis failure pathway is shown in Fig. 2, along with the neutral potential surface for comparison (critical structure energies denoted for the neutral and cation by ○ and ●, respectively). The relative

reaction enthalpies for cationic AlQ3 hydrolysis are listed in Table 1, along with inner coordination sphere bond lengths for the critical point structures. As seen in Fig. 2 and Table 1, the $AlQ3^+$ hydrolysis reaction products are calculated to be 22.0 kcal mol^{-1} higher in energy than the separated reactants, making the reaction roughly twice as endothermic as the neutral reaction pathway. The $AlQ3^+$ hydrolysis transition state has Al–O_a and H_2O O–H^1 bonds elongated by 0.41 and 0.02 Å compared to the cationic $AlQ3^+\cdots H_2O$ reactant complex. The Al–O distance decreases from 4.14 Å in the reactant complex, becoming 2.15 Å in the transition state, and the final product structure has an Al–O bond length of 1.72 Å. The effect of AlQ3 oxidation on the hydrolysis pathway barrier is quite significant. The $AlQ3^+$ activation energy is computed to be 15.7 kcal mol^{-1}, which is 8.5 kcal mol^{-1} lower than for the neutral process. The energy of the product species is stabilized in the product channel through formation of a $AlQ2OH^+\cdots HQ$ complex which is 11.2 and 17.5 kcal mol^{-1} lower in energy than the transition state and separated products, having an energy 4.5 kcal mol^{-1} higher than that of the reactants.

The local environment in the condensed phase can have a dramatic effect on activation energies and chemical reaction enthalpies. Experimental studies of the absorption and luminescence spectra of metal-quinolates in the condensed phase indicate that the monomers are weakly interacting.[33] This lends support for the use of AlQ3 monomers in quantum chemical studies of chemical reactivity. To check the validity of this approximation, polarizable continuum model (PCM) energy calculations were carried out to estimate the differences in energetics between the gas phase and in an AlQ3 thin solid film. In a PCM calculation, the reacting system is placed inside a cavity embedded in a polarizable continuum with a fixed dielectric constant characteristic of the condensed phase environment. Given the nature of the weakly interacting AlQ3 film, such an approach may be expected to be highly successful. The experimental dielectric constant of thin films of AlQ3 is reported to be 3.0 ± 0.3 as determined from capacitance measurements.[40] Using a dielectric constant of $\varepsilon = 3.0$ to represent the AlQ3 films, PCM calculations indicate that the effect on reaction energies is mostly small. The activation energy and endothermicity change by only 2.2 and −0.6 kcal mol^{-1} for neutral AlQ3, and 0.4 and −3.4 kcal mol^{-1} for cationic AlQ3 hydrolysis reactions, respectively, compared to the gas phase. It is notable though that the $AlQ3^+$ hydrolysis reaction becomes more thermodynamically favorable overall in the condensed phase.

During operation OLEDs can undergo significant heating due to the high resistance of the poorly conducting organic active layers (Joule effect). Joule heating has been implicated in the failure of AlQ3-based OLEDs, driving thermally activated processes such as changes in film morphology.[53,54] The absence of steady-state conditions during device operation and Joule heating of local sites in the AlQ3 active layer opens the potential for film degradation due to the AlQ3 hydrolysis pathway characterized here. If a typical value for the exponential prefactor is used (*ca.* 10^{14})[55] a rate constant of approximately 0.3 s^{-1} is obtained at 90 °C for the neutral AlQ3 reaction. Comparison of the relative reaction energetics for neutral and oxidized AlQ3, clearly suggests a role for charge imbalance in promoting chemical failure modes in OLED devices. The cationic AlQ3 hydrolysis reaction path is kinetically much more favorable than for the neutral case. The difference of *ca.* 8.5–10.3 kcal mol^{-1} in classical barrier heights (gas and condensed phase) results in the $AlQ3^+$ hydrolysis reaction being more than five orders of magnitude faster than the AlQ3 reaction.§

Conclusions

The reaction between a single molecule of H_2O and AlQ3 in both neutral and oxidized form has been investigated using hybrid density functional calculations as an initial attempt to model the degradation of OLEDs by trace amounts of water. Initially, neutral AlQ3 and H_2O form a reactant complex that is lower in energy by 5.3 kcal mol^{-1}, compared to the separated reactants. The hydrolysis pathway was found to be thermally activated, in agreement with experimental observations, having a classical barrier height of 24.2 kcal mol^{-1}. The final 8-hydroxyquinoline and neutral AlQ2OH products were determined to be higher in energy by 11.4 kcal mol^{-1}. Despite significant infrared spectral congestion, characteristic probes were identified to assist in the experimental corroboration of the role AlQ3 hydrolysis may play in OLED degradation. A comparison of electronic absorption between AlQ3 and AlQ2OH highlights clear differences in the spectra for these systems. Comparison of the reaction energetics calculated for neutral and oxidized AlQ3 clearly implicates charge imbalance in promoting the rate of chemical failure modes in OLED devices. The activation energy for the $AlQ3^+$ hydrolysis pathway is 35% lower than for AlQ3, making it significantly more kinetically favorable.

Acknowledgements

We gratefully acknowledge financial support from NSF (Grant No. CHE-0131157) and computational resources provided by NCSA (Grant No. CHE980042N). J. E. K. and H. P. H. would like to thank the Wayne State University, Institute for Scientific Computing for additional support provided by an NSF-IGERT Fellowship.

References

1 J. R. Sheats, H. Antoniadis, M. Hueschen, W. Leonard, J. Miller, R. Moon, D. Roitman and A. Stocking, *Science*, 1996, **273**, 884.
2 L. J. Rothberg and A. J. Lovinger, *J. Mater. Res.*, 1996, **11**, 3174.
3 J. H. Burroughes, D. D. C. Bradley, A. R. Brown, R. N. Marks, K. Mackay, R. H. Friend, P. L. Burns and A. B. Holmes, *Nature*, 1990, **347**, 539.
4 R. H. Friend, R. W. Gymer, A. B. Holmes, J. H. Burroughes, R. N. Marks, C. Taliani, D. D. C. Bradley, D. A. Dos Santos, J. L. Bredas, M. Logdlund and W. R. Salaneck, *Nature*, 1999, **397**, 121.
5 U. Mitsche and P. J. Bäuerle, *J. Mater. Chem.*, 2000, **10**, 1471.
6 C. W. Tang and S. A. VanSlyke, *Appl. Phys. Lett.*, 1987, **51**, 913.
7 Y. Hamada, *IEEE Trans. Electron Devices*, 1997, **44**, 1208.
8 B. C. Lin, C. P. Cheng, Z. Q. You and C. P. Hsu, *J. Am. Chem. Soc.*, 2005, **127**, 66.
9 M. D. Halls and H. B. Schlegel, *Chem. Mater.*, 2001, **13**, 2632.

§ $k_{AlQ3^+}/k_{AlQ3} \approx 1.3 \times 10^5$ to 1.6×10^6 at 90 °C (363 K) using gas and condensed phase energies in the Arrhenius relation.

10 J. P. Zhang and G. Frenking, *J. Phys. Chem. A*, 2004, **108**, 10296.
11 G. Gahungu and J. P. Zhang, *J. Phys. Chem. B*, 2005, **109**, 17762.
12 M. Amati and F. Lelj, *J. Phys. Chem. A*, 2003, **107**, 2560.
13 J. McElvain, H. Antoniadis, M. R. Hueschen, J. N. Miller, D. M. Roitman, J. R. Sheets and R. L. Moon, *J. Appl. Phys.*, 1996, **80**, 6002.
14 P. E. Burrows, V. Bulovic, S. R. Forrest, L. S. Sapochak, D. M. McCarty and M. E. Thompson, *Appl. Phys. Lett.*, 1994, **65**, 2922.
15 H. Aziz and G. Xu, *J. Phys. Chem. B*, 1997, **101**, 4009.
16 H. Aziz, Z. D. Popovic, N. X. Hu, A. M. Hor and G. Xu, *Science*, 1999, **283**, 1900.
17 F. Papadimitrakopoulos, X. M. Zhang, D. L. Thomsen and K. A. Higginson, *Chem. Mater.*, 1996, **8**, 1363.
18 K. A. Higginson, X. M. Zhang and F. Papadimitrakopoulos, *Chem. Mater.*, 1998, **10**, 1017.
19 F. Papadimitrakopoulos, X. M. Zhang and K. A. Higginson, *IEEE J. Sel. Top. Quantum Electron.*, 1998, **4**, 49.
20 M. S. Xu, J. B. Xu, E. Z. Luo and Z. Xie, *Chem. Phys. Lett.*, 2003, **374**, 656.
21 M. S. Xu and J. B. Xu, *Synth. Met.*, 2004, **145**, 177.
22 M. J. Frisch, G. W. Trucks, H. B. Schlegel *et al.*, *GAUSSIAN 03, (Revision B.2)*, Gaussian, Inc., Pittsburgh, PA, 2003.
23 A. D. Becke, *J. Chem. Phys.*, 1993, **98**, 5648.
24 J. P. Perdew, in *Electronic Structure of Solids*, ed. P. Ziesche and H. Eschrig, Akademie Verlag, Berlin, 1991.
25 P. C. Hariharan and J. A. Pople, *Theor. Chim. Acta*, 1973, **28**, 213.
26 M. M. Francl, W. J. Petro, W. J. Hehre, J. S. Binkley, M. S. Gordon, D. J. DeFrees and J. A. Pople, *J. Chem. Phys.*, 1982, **77**, 3654.
27 C. Peng, P. Y. Ayala, H. B. Schlegel and M. J. Frisch, *J. Comput. Chem.*, 1996, **17**, 49.
28 R. Krishnan, J. S. Binkley, R. Seeger and J. A. Pople, *J. Chem. Phys.*, 1980, **72**, 650.
29 T. Clark, J. Chandrasekhar and P. v. R. Schleyer, *J. Comput. Chem.*, 1983, **4**, 294.
30 R. E. Stratmann, G. E. Scuseria and M. J. Frisch, *J. Chem. Phys.*, 1998, **109**, 8218.
31 V. Barone and M. Cossi, *J. Phys. Chem. A*, 1998, **102**, 1995.
32 M. Cossi, N. Rega, G. Scalmani and V. Barone, *J. Comput. Chem.*, 2003, **24**, 669.
33 P. E. Burrows, Z. Shen, D. M. McCarty, S. R. Forrest, J. A. Cronin and M. E. Thompson, *J. Appl. Phys.*, 1996, **79**, 7991.
34 P. Addy, D. F. Evans and R. N. Sheppard, *Inorg. Chim. Acta*, 1987, **127**, L19.
35 G. P. Kushto, Y. Iizumi, J. Kido and Z. H. Kafafi, *J. Phys. Chem. A*, 2000, **104**, 3670.
36 A. Curioni, M. Boero and W. Andreoni, *Chem. Phys. Lett.*, 1998, **294**, 263.
37 A. Curioni and W. Andreoni, *J. Am. Chem. Soc.*, 1999, **121** 8216.
38 A. Curioni, W. Andreoni, R. Treusch, R. F. Himpsel, E. Haskal, P. Seidler, S. Kakar, T. van Buuren and L. J. Terminello, *Appl. Phys. Lett.*, 1998, **72**, 1575.
39 N. Johansson, T. Osada, S. Stafstrom, W. R. Salaneck, V. Parente, D. A. dos Santos, X. Crispin and J. L. Bredas, *J. Chem. Phys.*, 1999, **111**, 2157.
40 R. L. Martin, J. D. Kress, I. H. Campbell and D. L. Smith, *Phys. Rev. B: Condens. Matter*, 2000, **61**, 15804.
41 I. Fujii, N. Hirayama, J. Ohtani and K. Kodama, *Anal. Sci.*, 1996, **12**, 153.
42 H. Schmidbaur, J. Lettenbaur, D. L. Wilkinson, G. Müller and O. Kumberger, *Z. Naturforsch., B*, 1991, **46**, 901.
43 S. M. Smith and H. B. Schlegel, *Chem. Mater.*, 2003, **15**, 162.
44 M. D. Halls and H. B. Schlegel, *J. Chem. Phys.*, 1998, **109**, 10587.
45 A. P. Scott and L. Radom, *J. Phys. Chem.*, 1996, **100**, 16502.
46 T. A. Hopkins, K. Meerholz, S. Shaheen, M. L. Anderson, A. Schmidt, B. Kippelen, A. B. Padias, H. K. Halls, N. Peyghambarian and N. R. Armstrong, *Chem. Mater.*, 1996, **8**, 344.
47 H. B. Klevens and J. R. Platt, *J. Chem. Phys.*, 1949, **17**, 470.
48 H. H. Perkampus and K. Kortüm, *Zh. Anal. Khim.*, 1962, **190**, 111.
49 T. P. Nguyen, P. Jolinat, P. Destruel, R. Clergereaux and J. Farenc, *Thin Solid Films*, 1998, **325**, 175.
50 S. A. Van Slyke, C. H. Chen and C. W. Tang, *Appl. Phys. Lett.*, 1996, **69**, 2160.
51 Y. Hamada, T. Sano, M. Fujita, T. Fujii, Y. Nishio and K. Shibata, *Jpn. J. Appl. Phys.*, 1993, **32**, L514.
52 M. Probst and R. Haight, *Appl. Phys. Lett.*, 1997, **71**, 202.
53 J.-W. Choi, J. S. Kim, S. Y. Oh and W. H. Lee, *Mol. Cryst. Liq. Cryst. Sci. Technol., Sect. A*, 2001, **371**, 285.
54 T.-S. Kim, D.-H. Kim, H.-J. Im, K. Shimada, R. Kawajiri, T. Okubo, H. Murata and T. Mitani, *Sci. Technol. Adv. Mater.*, 2004, **5**, 331.
55 See, for example: R. I. Masel, *Principles of Adsorption and Reaction on Solid Surfaces*, Wiley, New York, 1996, p. 607.